

Short Communication

Fabrication of Nitrogen-Doped Carbon Nanofiber Networks for Oxygen Reduction Reaction

Shiming Meng, Mei Yu*, Jianhua Liu, Songmei Li

School of Materials Science and Engineering, Beihang University, Beijing 100191, China

*E-mail: yumei@buaa.edu.cn

Received: 3 March 2017 / Accepted: 29 March 2017 / Published: 12 May 2017

In this work, nitrogen-doped carbon nanofiber networks (NCFWs) were fabricated by a simple method of paralyzing polypyrrole nanofiber networks (PPy NFWs) precursor. Scanning electron microscopy (SEM), Transmission electron microscopy (TEM), X-ray diffraction (XRD) and Fourier transform infrared spectroscopy (FTIR) were employed to investigate the microstructure and composition of the as-prepared sample. Then the nitrogen-doped carbon nanofiber networks was further evaluated for its performance on Oxygen reduction reaction (ORR) with Cyclic voltammograms (CVs) and Linear sweep voltammograms (LSVs). The results showed that the fabricated NCFWs exhibited more remarkable catalytic performance compared with nitrogen-doped carbon nanoparticles (NFPs). Thus this material could be used as a better candidate in the field of fuel cells and metal-air batteries. The pyrolysis and structure of the NCFWs has obvious influence on their enhanced ORR properties.

Keywords: Oxygen reduction reaction; polypyrrole; networks; carbon; paralysis

1. INTRODUCTION

Oxygen reduction reaction (ORR) is generally considered as one of the most important processes in fuel cells, metal–air batteries, as well as other artificial energy conversion and storage systems[1, 2]. Pt and Pt-based alloys are the dominant electrocatalysts for ORR that have been widely investigated as effective candidate attributed to their superior activity and durability. Due to the disadvantage of its expensiveness, scarcity, and lack of durability, many studies have been performed in order to expose Pt-free ORR catalysts with high activity and durability [3-6]. In recent years, N-doped carbon nanomaterials as the promising candidates have been attracted great attention, and they show excellent ORR electrocatalytic activity since the nitrogen-doped active catalytic sites can facilitate the oxygen adsorption and decomposition of peroxide species [7]. Up to now, many efforts

have been devoted to exploring the methods to prepare N-doped carbon nanomaterials with different structures [8, 9].

Polypyrrole, containing high nitrogen content (~21wt %), exhibits plenty of excellent properties in terms of good stability, environmentally benign, excellent redox activity, and high proton conductivity. Besides the high nitrogen content, a high amount of carbonaceous residue can be achieved after pyrolysis. High-yield polypyrrole can be easily synthesized based on literature, making it industrially feasible [10]. Polypyrrole has already been used as a good catalyst for ORR and a good matrix for loading electrocatalytic nanoparticles [11]. Recently, many investigation have been conducted to explore the potential of polypyrrole-derived carbon as an anode material for Lithium-ion batteries [12], an adsorbent for CO₂ capture and a catalyst for CO₂ conversion [13]. In this work, nitrogen-doped carbon nanofiber networks (NCFWs) were fabricated by a two-step synthetic method. Firstly, polypyrrole nanofiber networks (PPy NFWs) were synthesized using a modified oxidative template assembly method, and then carbonized at 800 °C under an argon atmosphere. The ORR performance of the nitrogen-doped carbon nanofiber networks was evaluated by cyclic voltammograms (CVs) and linear sweep voltammograms (LSVs).

2. EXPERIMENTAL PROCEDURE

2.1. Materials

Pyrrrole monomer, Hexadecyl trimethyl ammonium Bromide (CTAB), concentrated hydrochloric acid (HCl, 36~38 wt%) and ammonium persulfate (APS, (NH₄)₂S₂O₈) were purchased from Sinopharm Chemical Reagent Co. Ltd.. Nafion (5wt %) was bought from DuPont. No in-house purification step were executed before the use of all the above analytical grade chemicals.

2.2. Fabrication of nitrogen-doped carbon nanofiber networks

A modified oxidative template assembly method was applied to synthesize PPy NFWs precursor as described in the literature[10]. Typically, a CTAB solution with the concentration of 50 mM was prepared by dissolving CTAB in a pre-cooled HCl solution (1 M). APS (9 mmol) and Pyrrole monomer (0.83 mL) were then added above the solution in sequence. PPy NFWs were obtained after keeping the solution in an ice bath (0~4°C) for 24 hours. The whole experiment process was completed in the ice bath (0~4°C). The PPy NFWs precipitate was washed to be neutral using deionized hot water and ethanol multiple times, and then dried at 60 °C in a vacuum oven for 24h.

The obtained PPy NFWs was heated at 800°C for 2h with a heating rate of 10 °C min⁻¹ under argon atmosphere in a quartz tubular furnace. After naturally cooling down to room temperature, the carbonized production were thoroughly washed with deionized water and ethanol and dried for 12h at 60 °C in an oven. For the sake of contrast, nitrogen-doped carbon nanoparticles (NFPs) was fabricated by the same reaction conditions of paralyzing polypyrrole nanoparticles precursor.

2.3. Instrumentations and characterizations

The morphology and microstructure of the products were observed by transmission electron microscope (TEM, JEOL2100F), equipped with a field emission gun operating at 200 kV, and scanning electron microscope (FE-SEM, JEOL JSM-7500). The crystallographic structures of the samples were characterized by X-ray diffractometer (XRD, Rigaku D/max-2200PC) using CuK radiation ($\lambda= 1.5418\text{\AA}$) operated at 200 mA and 40 kV in the diffraction angle range 10–80°. The infrared spectra (IR) were recorded on a Bruker IFS 66V/S FTIR spectrometer by dispersing the samples in potassium bromide pellets, from 4000 to 400 cm^{-1} wave numbers.

Electrochemical measurements were performed using a VersaSTAT VMC electrochemical analyzer with a conventional three-electrode cell at room temperature. A graphite rod electrode and an Ag/AgCl electrode filled with saturated KCl aqueous solution were used as the counter and reference electrodes. The electrocatalytic activity toward ORR was measured in O₂-saturated 0.1 M KOH solution using a glassy carbon rotating disk electrode loading the catalysts. The measured materials (3 mg) were predispersed in the mixture solution of 40 μL 5wt% nafion solution and 1000 μL dehydrated ethanol by ultrasonication for 30 min. A 40 μL portion of the as-prepared ink was dropped on the surface of the glassy carbon, yielding a working electrode with a loading of 0.5 mg cm^{-2} after air-drying. Cyclic voltammetry (CV) tests were measured within a voltage range from 0.2 to -1.2 V (vs. Ag/AgCl electrode) at a scan rate of 100 mV/s. The Linear sweep voltammetry (LSV) curves of different samples were recorded at various rotation speeds ranging from 100 to 2025 rpm with a scan rate of 5 mV s^{-1} in 0.1 M KOH solution that was purged with O₂ flow all through.

3. RESULTS AND DISCUSSION

3.1. Morphology and composition of the NCFWs

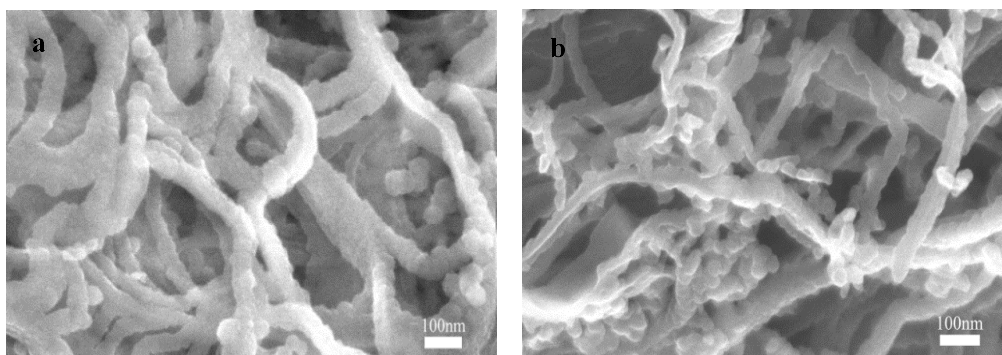


Figure 1. FE-SEM images of PPy NFWs (a) and NCFWs, (b) A network structure is observed in both samples. The scale bars in both images represent 100 nm

As shown in Fig.1, the PPy NFWs precursor is in a 3D network structure composed of the nanofibers with the average diameter of ~ 100 nm. The large surface area of the structure ensures the precursor to be carbonized uniformly, thereby producing a well-structured network. The resultant

carbon samples, as shown in Figure 1b, also exhibited a cross-linked nanofiber structure, which is very similar to the PPy NFWs precursor, but with shrined nanofiber diameters. The surface texture of the fibers is rougher than the precursor, which favors the contact of the active basic sites with surrounded ions during ORR reactions. Numbers of small aggregated fragments of the nanofibers were formed attributed to the high activation temperature.

With the purpose of further understanding the detailed morphology and structure of the NCFWs, its representative sample were investigated with Transmission electron microscopy. Based on the TEM images in Figure 2a, the cross-linked structure and roughness of the nanofibers surface is confirmed. Combined with the SEM images, such a conclusion can be draw that if the PPy NFWs precursor could be directly carbonized at 800°C, the as-synthesized samples could almost maintained the whole morphology of the precursor network. In addition, the selected area electron diffraction (SAED) pattern of the sample was also taken to confirm the existence of the disordered carbon structure. This result fits well with the XRD patterns as shown in Fig. 3a.

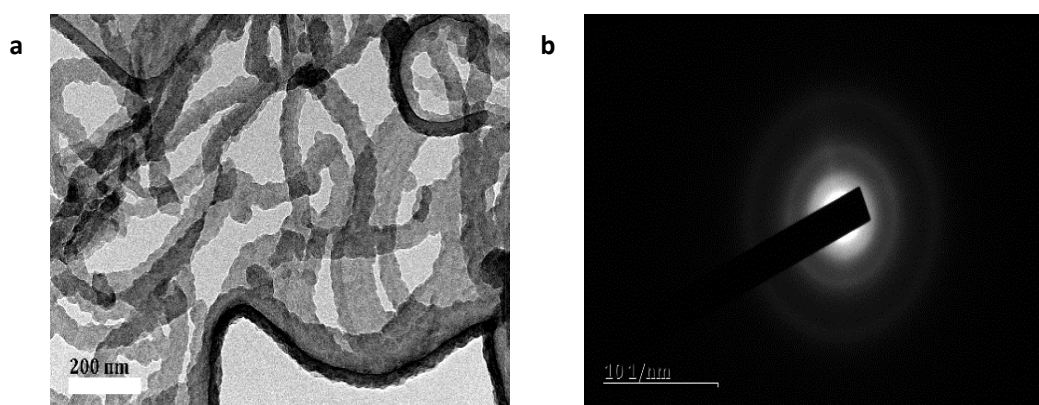


Figure 2. (a) TEM images of the NCFWs, (b) SAED pattern

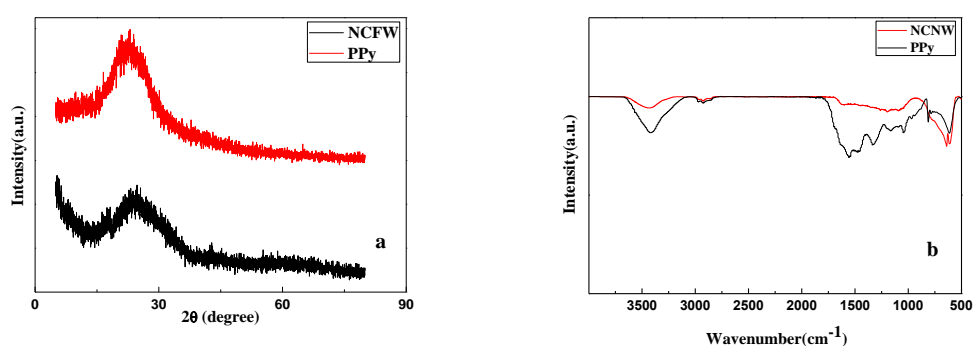


Figure 3. X-ray diffraction patterns (a), FTIR spectra (b)

Figure.3a shows the XRD patterns of the PPy NFWs and NCFWs. Both of the patterns exhibit one broad characteristic peaks. For NCFWs, the peak at around 26° corresponded to (002) reflection of graphite[10]. This suggests that NCFWs sample has disorderly oriented graphitic type fragments in its structure. At the same time, it exhibited low degree of graphitization.

The chemical bonding information and the nature of the nitrogen functionalities of the sample was investigated with Fourier transform infrared spectroscopy (FTIR). Figure 3b shows the FTIR spectra of the PPy NFWs and NCFWs. The FTIR spectrum of PPy NFWs exhibits well-defined characteristic peaks of this polymer [14]. The broad band at 3420 cm^{-1} is attributed to the N-H and/or O-H symmetric stretching vibration, and the weak bands at around 2900 and 2850 cm^{-1} was believed to be caused by asymmetric and symmetric C-H stretching vibration. The C-C stretching vibration and C-N stretching vibration result in the peaks at 1590 and around $1370\text{-}1250\text{ cm}^{-1}$, respectively. In the carbonized samples, broader and overlapping bands are formed, which can be explained by the strong absorption of carbon, while the less intensity of the bands indicates the presence of nitrogen species [15]. It should be noted that the intensity of the band corresponding to the stretching vibrations of N-H and/or O-H groups declines, indicating the groups are disappearing during carbonization. The same conclusion can be drawn for C-N stretching vibrations, in-plane and out-of-plane C-H and N-H deformations through the peaks at $1360\text{-}800\text{ cm}^{-1}$ decreases. According to the results, N-H and C-N species still exist in the NCFWs samples.

3.2. Electrochemical measurement of the NCFWs

Oxygen reduction reaction occurs mainly through two ways in alkaline solution, as shown in the following equations:

(1) 4e process :



(2) 2e process :

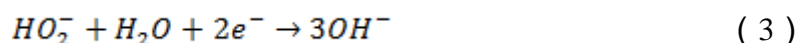
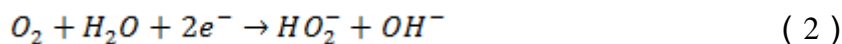


Fig.4a shows the Cyclic voltammograms of NCPs and NCFWs in the O_2 -saturated 0.1 M KOH solution. Both catalysts exhibit a well-defined cathodic ORR peaks located in the potential range between -1.2 and 0.2 V . NCFWs shows the peak potential at -0.21 V more positive than NCPs. Moreover, the current density corresponding to the reduction peak of NCFWs is also higher than that of NCPs.

Furthermore, the RDE measurement was performed to investigate the ORR activity of the prepared electrode. In contrast, the ORR activities of NCPs were also measured. As clearly shown in Fig.4b, NCPs and NCFWs exhibit different ORR performances. The values of onset potential for them are -0.26 and -0.13 V , respectively. The NCFWs electrode shows the more positive onset potential and the larger current, which indicates the better ORR activity than NCPs [16]. Fig.4c shows the RDE voltammograms for ORR of NCFWs at different rotation speeds from 100 to 2025 . These polarization curves show typical increasing current with increased rotating speeds, which were caused by that high rotating rates quicken oxygen flux to the electrode surface [17, 18]. Fig.4d shows the K-L plots at the potential of -0.8 V for NCPs and NCFWs. The plots of both samples exhibit good linearity. The

electron transfer numbers (n) of NCPs and NCFWs are 3.56 and 3.96, respectively, by the calculation of the formula, indicating a major four electron ORR pathway on both electrodes [19]. It is clearly that NCFWs have a larger electron transfer number, which may benefit from the 3D structure and more uniform carbonization process [20]. The experimental results indicated that NCFWs has a 3D structure with interconnected networks, which is propitious to provide fast ionic channels for ORR. The obtained NCFWs have the approximately four-electron(4-e) transfer processes and high current density, making it a possible nonprecious metal catalyst for ORR.

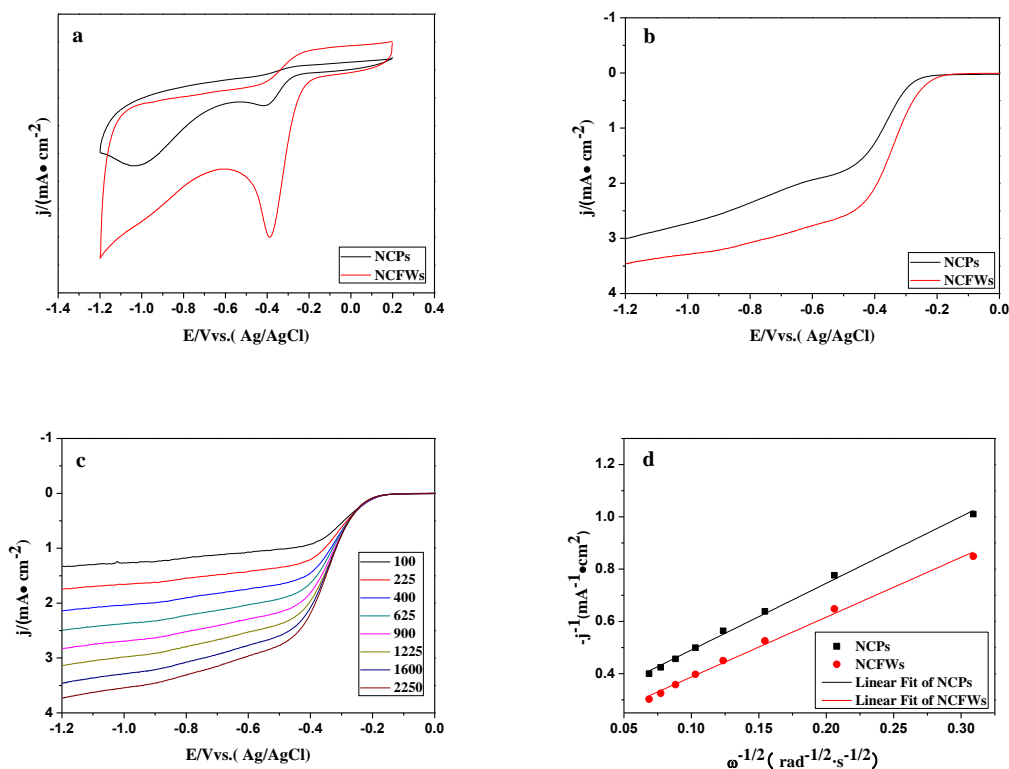


Figure 4. (a) CV curves of the NCPs and NCFWs electrode, (b) RDE voltammograms in the O₂ saturated 0.1 M KOH electrolyte (rotation speed 1600 rpm, scan rate 10 mV/s) for NCPs and NCFWs, (c) RDE voltammograms for ORR on the NCFWs electrode at different rotation speeds, (d) K-L plots (i^{-1} vs. $\omega^{-1/2}$) at the potential of -0.8 V for NCPs and NCFWs.

4. CONCLUSIONS

In summary, PPy nanofiber networks, which were obtained by in-situ polymerization of pyrrole monomers, have been proven to be a very effective precursor for preparing NCFWs by simple pyrolysis. The resulting NCFWs as an ORR electrocatalyst exhibits remarkable catalytic performance comparable to the NCPs, making it a promising candidate for potential usage in the fields of fuel cells and metal-air batteries. Moreover, the intrinsic 3D structure of NCFWs can serve as a tunable platform hierarchically integrating cocatalyst.

ACKNOWLEDGEMENTS

This work is supported by the National Natural Science Foundation of China (Project No. 21371019).

References

1. I. Katsounaros, S. Cherevko, A. R. Zeradjanin and K. J. J. Mayrhofer, *Angew. Chem. Int. Edit.*, 53 (2014) 102.
2. X. G. Li, B. N. Popov, T. Kawahara and H. Yanagi, *J. Power Sources*, 196 (2011) 1717.
3. X. Q. Huang, Z. P. Zhao, L. Cao, Y. Chen, E. B. Zhu, Z. Y. Lin, M. F. Li, A. M. Yan, A. Zettl, Y. M. Wang, X. F. Duan, T. Mueller and Y. Huang, *Science*, 348 (2015) 1230.
4. Y. J. Wang, N. N. Zhao, B. Z. Fang, H. Li, X. T. T. Bi and H. J. Wang, *Chem. Rev.*, 115 (2015) 3433.
5. Y. C. Xin, J. G. Liu, Y. Zhou, W. M. Liu, J. A. Gao, Y. Xie, Y. Yin and Z. G. Zou, *J. Power Sources*, 196 (2011) 1012.
6. N. Daems, X. Sheng, I. F. J. Vankelecom and P. P. Pescarmona, *J. Mater. Chem. A*, 2 (2014) 4085.
7. P. Chen, L. K. Wang, G. Wang, M. R. Gao, J. Ge, W. J. Yuan, Y. H. Shen, A. J. Xie and S. H. Yu, *Energy Environ. Sci.*, 7 (2014) 4095.
8. G. Nam, J. Park, S. T. Kim, D. B. Shin, N. Park, Y. Kim, J. S. Lee and J. Cho, *Nano Lett.*, 14 (2014) 1870.
9. G. L. Tian, M. Q. Zhao, D. S. Yu, X. Y. Kong, J. Q. Huang, Q. Zhang and F. Wei, *Small*, 10 (2014) 2251.
10. Y. Li, B. Zou, C. Hu and M. Cao, *Carbon*, 99 (2016) 79.
11. M. Salehi and M. Saremi, *Int. J. Electrochem. Sci.*, 9 (2014) 1497.
12. T. Yuan, Y. S. He, W. M. Zhang and Z. F. Ma, *Chem. Commun.*, 52 (2016) 112.
13. M. Sevilla, P. Valle-Vigón and A. B. Fuertes, *Adv. Funct. Mater.*, 21 (2011) 2781.
14. P. A. Palod and V. Singh, *Sensors Actuat. B- Chem.*, 209 (2015) 85.
15. G. Ćirić-Marjanović, S. Mentus, I. Pašti, N. Gavrilov, J. Krstić, J. Travas-Sejdic, L. T. Strover, J. Kopecká, Z. Moravková, M. Trchová and J. Stejskal, *J. Phys. Chem. C*, 118 (2014) 14770.
16. C. D Bari, A. Goni-Urtiaga, M. Pita, S. Shleev, M. D. Toscano, R. Sainz and A. L. D. Lacey, *Electrochim. Acta*, 191 (2016) 500.
17. S. Lee, D. H. Kwak, S. B. Han, E. T. Hwang, M. C. Kim, J. Y. Lee, Y. W. Lee and K. W. Park, *Electrochim. Acta*, 191 (2016) 805.
18. D. Morales-Acosta, F. J. Rodriguez-Varela and R. Benavides, *Int. J. Hydrog. Energy*, 41 (2016) 3387.
19. G. Nam, J. Park, S. T. Kim, D. B. Shin, N. Park, Y. Kim, J. S. Lee and J. Cho, *Nano Lett.*, 14 (2014) 1870.
20. A. Morozan, P. Jegou, S. Campidelli, S. Palacin and B. Josselme, *Chem. Commun.*, 48 (2012) 4627.